

The Importance of Slag Engineering in Freeze-Lining Applications

MIEKE CAMPFORTS, BART BLANPAIN, and PATRICK WOLLANTS

Freeze linings are frequently used to protect the reactor wall in pyrometallurgical processes. In order to minimize reactor wall corrosion, the stability of a freeze lining has to be guaranteed. To illustrate the importance of slag engineering in the optimization of freeze-lining behavior, the freeze-lining formation of six synthetic lead slags is studied. Lab-scale freeze linings are obtained using a cooled-probe technique and their microstructures are characterized using light optical microscopy (LOM) and microprobe analysis. The results show that slag engineering can have a major impact on the operative freeze-lining formation mechanisms. Some slag properties found to affect the freeze-lining formation are the viscosity, the temperature stability range of the relevant phases, the type of phases that form (interlocking or not), and the crystallization behavior of the slag. The operational demands of a protective freeze lining are defined by the authors as follows: (1) a rapid formation to limit the contact between the reactor wall and the corrosive bath material and (2) a sufficient stability during changes in heat input from the bath and in bath composition. From the comparison of the microstructural features of the freeze linings formed with the studied slags, it is concluded that these demands can be fulfilled with the growth of an initial layer dominated by the presence of interlocking crystals in combination with the subsequent formation of a high-melting crystalline layer at the bath–freeze-lining interface, which is in equilibrium with the slag bath and the composition of which differs sufficiently from the bath composition.

DOI: 10.1007/s11663-009-9258-7

© The Minerals, Metals & Materials Society and ASM International 2009

I. INTRODUCTION

FREEZE linings are extensively used to protect refractory walls from corrosion. A major advantage of the freeze-lining concept is that the freeze lining consists of solidified process material and, therefore, is self-regenerating and can resist aggressive process materials. To apply the freeze-lining concept in a reactor, its formation and its stability have to be assured. As a result, it is important to control the freeze-lining behavior.

In previous research, the freeze-lining behavior was often studied in modeling work^[1–3] or in experimental observations of the freeze-lining microstructure^[4,5] while considering the composition of the process material as fixed. However, for the zinc fuming process, Verscheure *et al.* showed that a proper selection of bath composition and the corresponding liquidus temperature minimize the heat loss and improve the process output.^[6,7] For slag splashing,^[8] it was indicated that the freeze-lining behavior can be improved by adjusting the slag composition and splashing temperature to obtain a

proper ratio between high-melting and low-melting phases. The high-melting phases protect the refractory from corrosion, while the low-melting phases attach the high-melting phases to the refractory. Also, in the studies of the microstructure evolution of an industrial nonferrous slag^[9,10] and a synthetic lead slag,^[11,12] slag properties such as the temperature stability range of a phase, the type of phase dominating the freeze-lining microstructure (forming a closed structure or not, interlocking or not), the crystallization behavior, and the mass transfer are suggested to affect the freeze-lining formation. Thus, when optimizing the freeze-lining behavior, changes in process parameters, such as the composition of the process material and the process temperature, also have to be considered. Thus, the process material can be adapted to optimize both the freeze-lining formation and the process output.

In the present article, the authors explore the freeze-lining formation of six different slags to illustrate the importance of slag engineering for a freeze lining in continuous contact with the slag bath. Furthermore, microstructural characteristics of a protective freeze lining are indicated and the freeze-lining formation of the six slags is evaluated accordingly.

II. EXPERIMENTAL

A. Cooled-Probe Technique

In previous experiments, a water-cooled probe technique was used, as is described extensively

MIEKE CAMPFORTS, formerly Research Assistant, Materials Science Department, Katholieke Universiteit Leuven, is Project Leader, Umicore Research, 2250 Olen, Belgium. Contact e-mail: mieke.campforts@eu.umicore.com BART BLANPAIN and PATRICK WOLLANTS, Professors, are with the Centre for High Temperature Processes, Metallurgy and Refractory Materials, Department of Metallurgy and Materials Engineering, Katholieke Universiteit Leuven, 3001 Leuven, Belgium.

Manuscript submitted February 13, 2009.

Article published online July 22, 2009.

elsewhere.^[9,10,13] In the present experiments, air cooling was applied, to limit the cooling of the bath after submerging the probe, and an adapted thermocouple setup was used (Reference 12), which measures the temperatures at 1 and 2 cm from the probe and in the bath at approximately 3 to 4 cm underneath the probe. The experimental procedure is as follows: 3 kg of mixed pure oxide powders are melted in an Al₂O₃ crucible in open air. When the targeted bath temperature of 1240 °C is reached, an initial bath sample is taken with a cold steel rod and quenched in water. Next, the air-cooled probe with two thermocouples fixed at 1 and 2 cm from the probe is submerged 30 mm into the bath during 1, 5, 15, 30, 60, and 120 minutes to form a freeze layer, while the rotational speed of the crucible (28.5 rpm), air-flow rate (25 Nm³/h), and bath temperature (1240 °C) are kept constant. At the end of the experiment, the probe is taken quickly from the bath and the freeze layer is quenched in water. Similar to the initial bath sample, a final bath sample is taken.

B. Analysis

All samples are analyzed using light optical microscopy (LOM) and electron probe microanalysis (EPMA). An EPMA using wavelength-dispersive spectroscopy is performed with a reference current of 30 nA, using the willemite standard of a 20-kV acceleration voltage. As standards, anglesite, willemite, and hematite are used for Pb, Zn, and Fe, respectively, and glaverbel glass is used for Al, Si, and Ca. The bath samples of S1 are analyzed with X-ray fluorescence spectroscopy (XRF) using UniQuant* software. The

*UniQuant is the trademark of Thermo Fisher Scientific Inc., Rockford, IL.

XRF analyses are performed using a 4-kW Rh tube.

C. Thermodynamic Calculations

Thermodynamic calculations are performed with FactSage,^[14] using the FACT53 and FACToxid thermodynamic databases developed for the Pb- and Zn-containing slag systems.^[15,16] All calculations are performed for a system in equilibrium with air, because no reduction agent is present and the slag is continuously in contact with air.

Table I. Target Composition of Synthetic Lead Slags (Weight Percent)

| Slag | CaO | SiO ₂ | PbO | ZnO | Fe ₂ O ₃ | Al ₂ O ₃ |
|------|------|------------------|------|-----|--------------------------------|--------------------------------|
| M1 | 12.0 | 11.0 | 48.0 | 4.0 | 22.0 | 3.0 |
| M2 | 11.7 | 16.3 | 50.5 | 8.3 | 13.2 | 0.0 |
| M3 | 17.0 | 26.0 | 39.0 | 5.5 | 10.5 | 2.0 |
| S1 | 4.0 | 11.0 | 58.5 | 3.5 | 20.5 | 2.5 |
| S2 | 13.3 | 22.4 | 44.8 | 5.7 | 11.3 | 2.5 |
| S3 | 8.0 | 25.3 | 50.5 | 4.1 | 9.5 | 2.5 |

D. Slag

Six synthetic lead slags are made by melting pure oxide powders (less than 0.1 wt pct impurities). CaO is added as CaCO₃. The targeted slag compositions are shown in Table I. The slag compositions are altered to obtain a liquidus temperature predicted to be 1200 °C, melilite or spinel as the primary phase (Mx or Sx, respectively), and a change in SiO₂ concentration to affect the viscosity of the slags.

III. RESULTS

A. Temperature Measurements

Figure 1 shows the temperature measurements for the 120-minute experiments. For all slags, the bath temperature fluctuates around the target temperature of 1240 °C. For only the first 15 to 30 minutes is a rather strong deviation sometimes observed (*e.g.*, for M2). The temperature at 2 cm from the probe follows the bath temperature closely. For M1 and M3 only, after 60 minutes, the temperature at 2 cm from the probe starts to decrease below the bath temperature and to reach a temperature of 1170 °C and 1160 °C, respectively, at 120 minutes. The temperature at 1 cm from the probe for all slags immediately drops 100 °C to 200 °C after the probe is submerged. Thereafter, for M2, S1, and S3, this temperature stabilizes after 15 to 40 minutes at 1130 °C, 860 °C, and 1050 °C, respectively. For S2, this temperature slightly decreases to 1050 °C. For M1 and M3, this temperature keeps decreasing to finally reach 900 °C and 925 °C, respectively. Note that, if the bath temperature fluctuates, similar fluctuations are observed for the other two temperatures.

B. Freeze-Lining Samples

1. Thickness of the freeze lining

Figures 2(a) and (b) show the freeze-lining thickness as a function of time for Mx and Sx, respectively. The M1 and M2 slags form a layer of approximately 10 mm within 15 minutes. The freeze lining of M2 seems to have reached its steady-state thickness after 120 minutes, while the freeze lining of M1 seems to be still growing. The freeze-lining thickness of M3 initially stabilizes at 5 mm, but after 60 minutes, this layer grows further. The steady-state thickness does not seem to be reached after 120 minutes. The S1 rapidly forms a freeze lining of 6 mm thickness in the first 5 minutes. After 5 minutes, the freeze lining grows gradually to fluctuate around 10 mm between 30 and 120 minutes. It is not clear if steady state is reached for this slag. The S2 forms a layer of 3.5 mm in the first minute, stagnates at approximately 6 mm between 30 and 60 minutes, and thereafter grows further to obtain a thickness of 8 mm at 120 minutes. For S3, the thickness of the 1- and 5-minute freeze linings could not be determined, because they immediately cracked into small pieces upon quenching. At 15 minutes, the freeze lining has reached a thickness of 4 mm. Thereafter, the layer grows very slowly to attain a constant thickness of 6 mm after

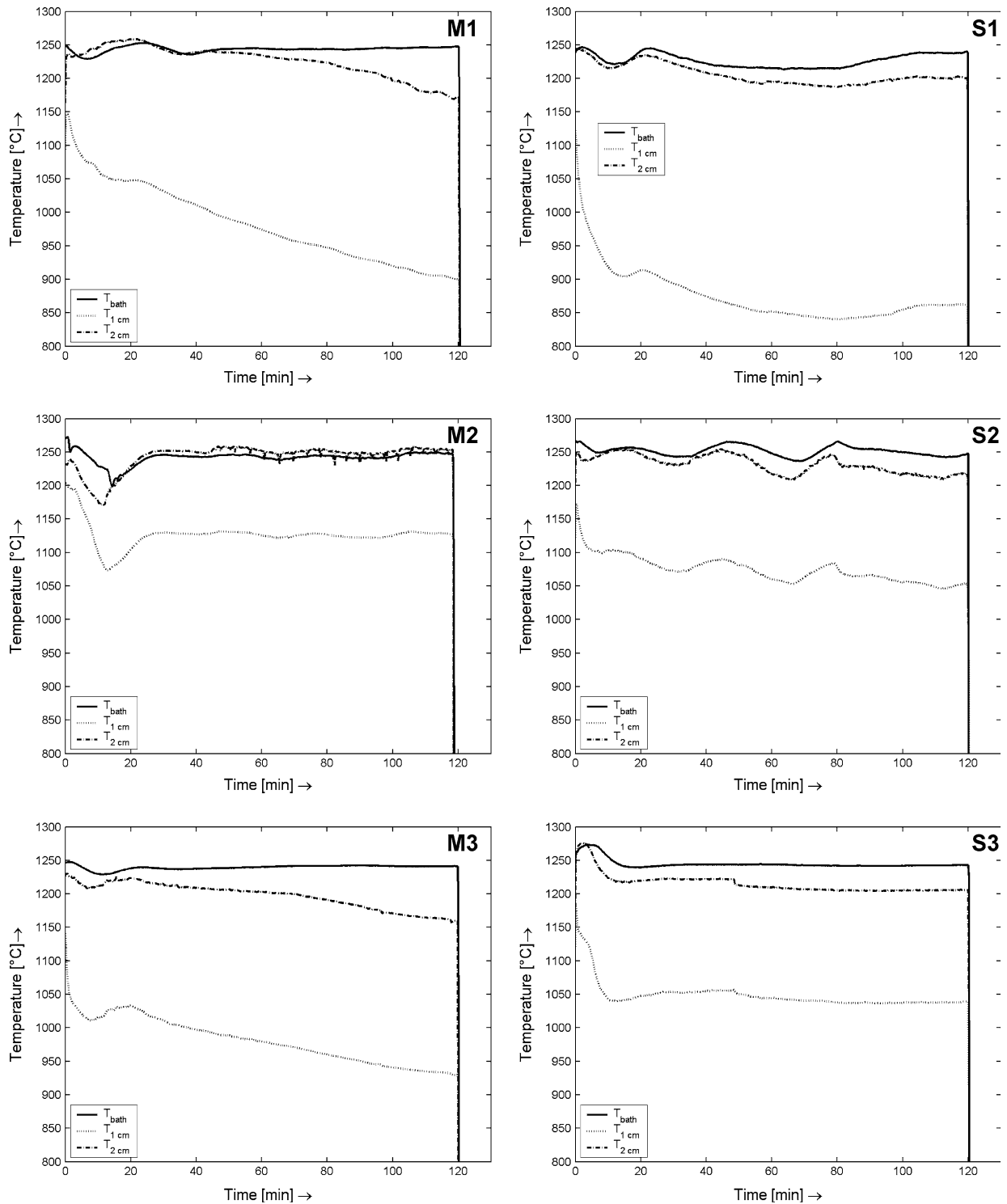


Fig. 1—Temperature evolution during the 120-min experiments of the slags with T_{bath} the bath temperature and $T_{1 \text{ cm}}$ and $T_{2 \text{ cm}}$ the temperature in the slag at 1 and 2 cm, respectively, from the probe.

60 minutes. For this slag, the steady-state thickness seems to be reached. Note that Sx, on average, forms thinner freeze linings than Mx and that, for both Mx and Sx, the final freeze-lining thickness increases with a decreasing SiO_2 -concentration.

2. Microstructure of the freeze lining

First, some general remarks need to be made. Before quenching, the samples of the glass phase in the microstructures were liquid or glass. If possible, a distinction is made between glass and liquid at high

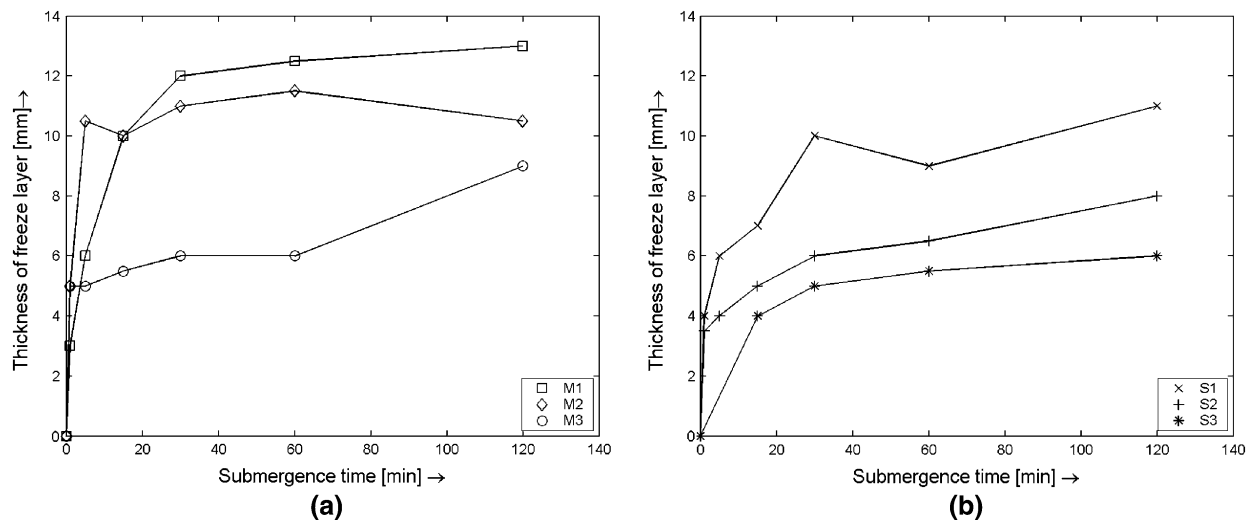


Fig. 2—Freeze-lining thickness as a function of time.

Table II. Numbers, Names, and Microstructural Characteristics of Layers in Freeze Linings and the Slags for Which the Layers Were Observed

| Layer | Name | Microstructural Characteristics | Slags |
|-------|------------------------------------|--|----------------|
| (1) | glass layer | only glass phase is observed | Mx and Sx |
| (2) | glass-with-crystals layer | equiaxed crystals are present in the glass phase | M1, M2, and Sx |
| (3) | crystalline layer | slag is fully crystalline | M1, M2, and S1 |
| (4) | (first) “crystals-in-liquid layer” | crystals are interlocked and contain liquid in between | Mx, S1, and S2 |
| (5) | sealing-crystals layer | large broad crystals that form a dense layer | M1, M2, and S2 |
| (6) | entrained-slag-bath layer | similar to the glass layer but located at the bath side of the freeze lining | Mx and Sx |
| (7) | second crystals-in-liquid layer | crystals are interlocked and contain liquid in between | M1 |

temperature by studying the change in the glass composition and in the crystal size with distance to the probe, as was also done in Reference 11. The term glass phase refers to both high-viscosity liquid and glass (for example, in the names of the layers in the freeze lining). When crystals are present, the order of crystal formation is determined by analyzing which crystals entrap others. For example, if spinel crystals are entrapped by melilite crystals (the spinel crystals are (partly) surrounded by melilite phase), the spinel crystals are thought to have formed first. Some crystal names are abbreviated: PCSi is short for $Pb_3(Ca,Pb)_2Si_3O_{11}$, PbFe for $PbFe_{10}O_{16}$, and PbFe-Si? for a phase for which the exact chemical formula could not be determined because its crystals are too small. Also, in the freeze-lining microstructures, up to seven layers are distinguished. These layers are defined in Table II and, in the text, the numbers of the layers refer to the numbers in the table.

The 5-, 60-, and 120-minute microstructures of M1 are shown in Figure 3. At 60 minutes, all seven layers ((1) through (7)) mentioned in Table II are distinguished. Layers (1) and (2) are observed in all microstructures. The crystals in layer (2) consist of melilite, spinel, PbFe, and PCSi phase. From 5 minutes, layer (3) is observed between layers (2) and (4). This layer (3) contains, in order of formation, melilite, spinel, PbFe, and PCSi crystals. Layer (4) is observed in all

microstructures. Until 30 minutes, this layer (4) is in contact with the bath. The order of phase formation differs with the position. At the probe side, melilite formed before spinel; at the bath side, it is the other way around. Nevertheless, melilite crystals always dominate the microstructure. PbFe formed third and PCSi last. After 30 minutes, large spinel and melilite crystals are present at the bath–freeze-lining interface, forming layer (5). At the probe side, this layer (5) is dominated by melilite crystals; at the bath side, it is dominated by spinel crystals. At 120 minutes, PbFe crystals are also observed. Layer (5) is in contact with the bath before 60 minutes, but at 60 minutes, layer (7) has formed. In this layer (7), spinel crystals form before melilite crystals. The morphology of the melilite crystals differs from the one in layer (4). Note that, at the probe side of layer (7), the fraction of glass phase is high and that, with time, PbFe crystals also appear here. A thin layer (6) is observed in all microstructures before 120 minutes; this layer contains glass phase and, at 60 minutes, also some small melilite and spinel crystals.

For M2, six layers ((1) through (6)) are distinguished at 120 minutes (Figure 4). These layers form in the same order as for M1. Layer (2) is observed in all microstructures, while layer (3) is observed from 5 minutes. Both layers contain, in order of formation, spinel, melilite, PCSi, and PbFe-Si? crystals. At 1 and

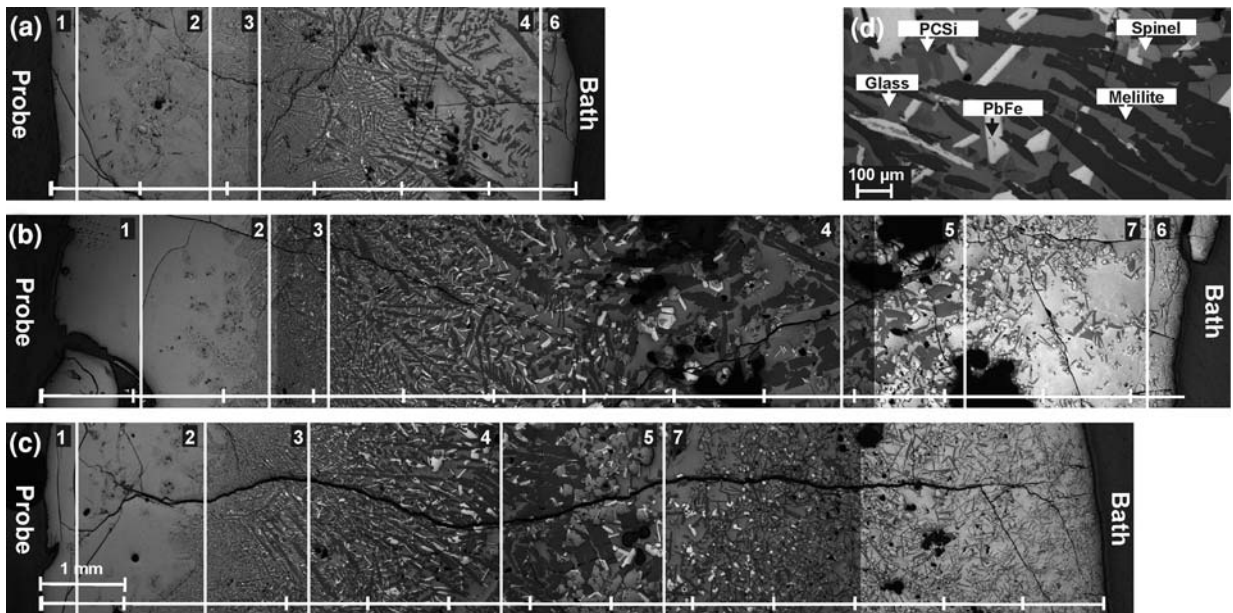


Fig. 3—LOM image of the freeze-lining microstructure of M1 after (a) 5, (b) 60, and (c) 120 min. Seven layers ((1) through (7)) can be observed. Fig. 3(d) shows a detail of the microstructure of layer (4) for 120 min, where the melilite, spinel, PbFe, PCSi, and glass phases are indicated. The scale bars indicate the distance to the probe.

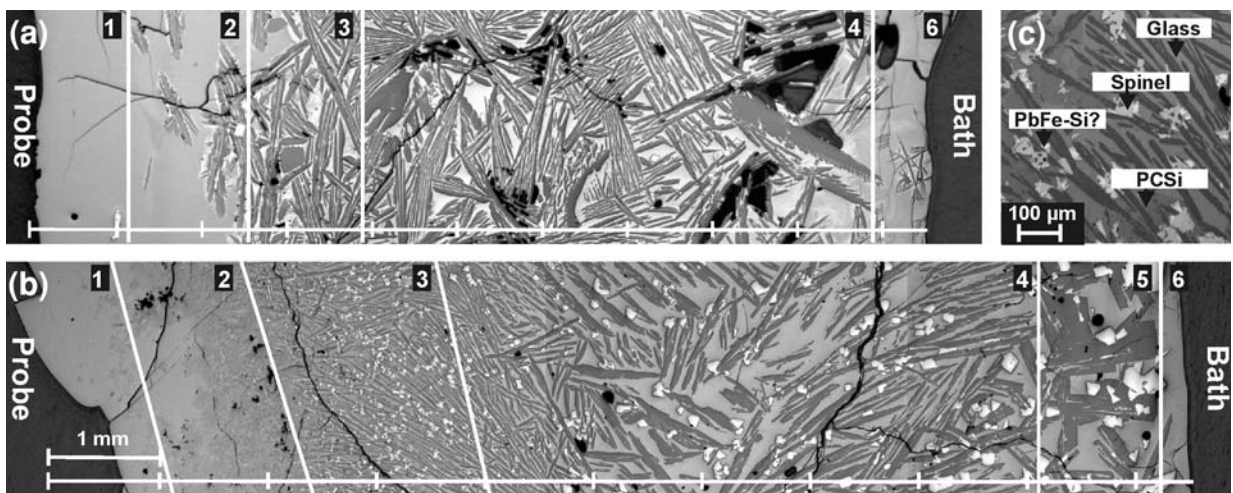


Fig. 4—LOM image of the freeze-lining microstructure of M2 after (a) 5 and (b) 120 min. Six layers ((1) through (6)) can be observed. Figure 4(c) shows a detail of the microstructure of layer (3) for 120 min, where the melilite, spinel, PbFe-Si?, PCSi, and glass phases are indicated. The scale bars indicate the distance to the probe.

5 minutes, layer (4) contains only melilite and spinel crystals. After 15 minutes, PCSi and PbFe-Si? crystals are observed at the bath side. In layer (5), broad and large melilite and large spinel crystals are observed. The size of these crystals increases with the experiment time. In layers (3) through (5), melilite crystals dominate the microstructure.

At 120 minutes, three layers ((1), (4), and (6)) are distinguished in the microstructure of M3 (Figure 5(b)). Until 60 minutes, only layers (1) and (6) are observed, as is shown for 15 minutes in Figure 5(a). The interface between these layers could not be determined. At 120 minutes, layer (4) is observed. The crystals consist

of melilite phase and, at the probe, some spinel and PbFe crystals are also observed. Because melilite forms dendrites and the freeze-lining thickness clearly increases after the crystals are formed (Figure 2(a)), they are assumed to grow in liquid. Perhaps at the probe side of layer (4), some high-viscosity liquid is present.

For S1 at 120 minutes, five layers ((1) through (4) and (6)) are distinguished in the microstructure (Figure 6(b)). A thin layer (1) is present in all microstructures. Sometimes spinel crystals are observed in this layer (1). Layer (2) is observed in all microstructures and contains small spinel, PbFe, and PCSi crystals. Layer (3) is only observed after 30 minutes. This layer contains, in

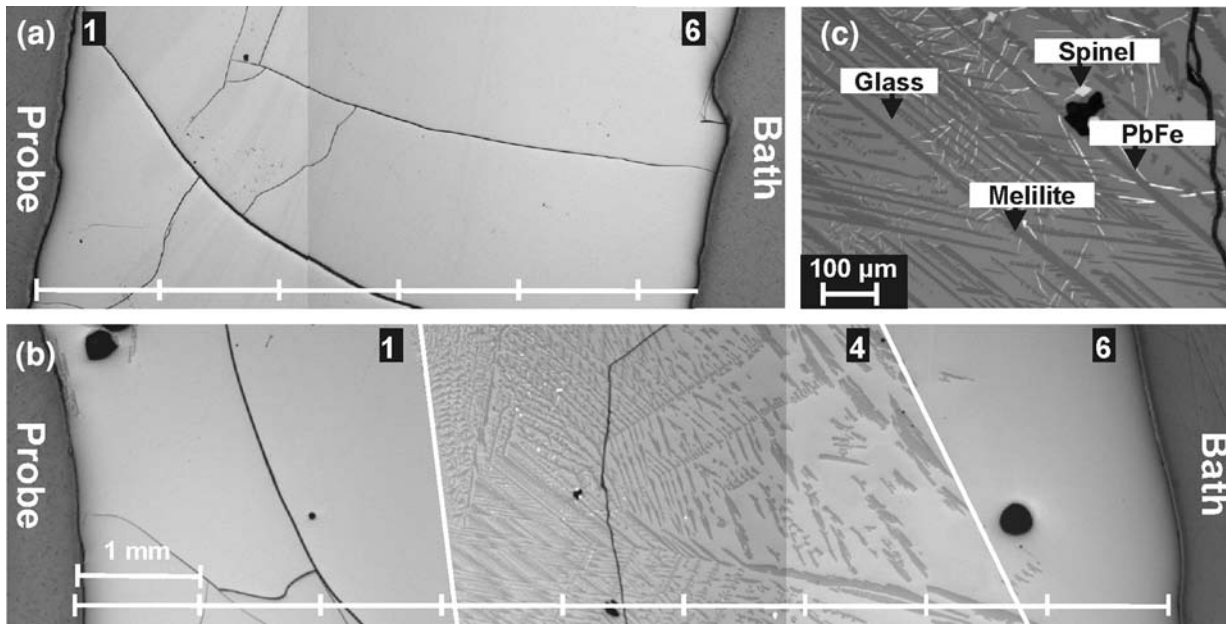


Fig. 5—LOM image of the freeze-lining microstructure of M3 after (a) 15 and (b) 120 min. Three layers ((1), (4), and (6)) are observed. Figure 4(c) shows a detail of the microstructure of layer (4) for 120 min, where the melilite, spinel, PbFe, and glass phases are indicated. The scale bars indicate the distance to the probe.

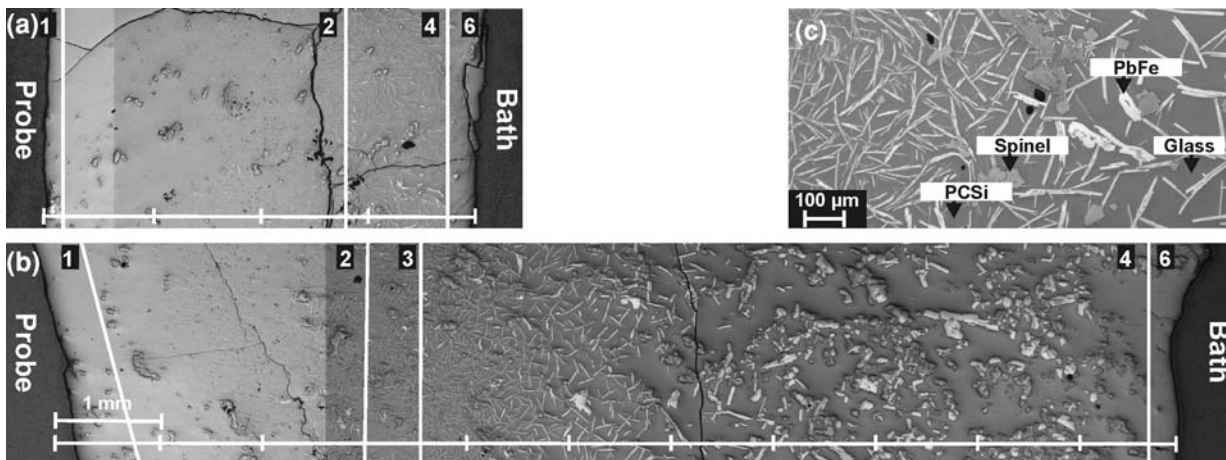


Fig. 6—LOM image of the freeze-lining microstructure of S1 after (a) 5 and (b) 120 min. Five layers ((1) through (4), and (6)) are observed. Figure 6(c) shows a detail of the microstructure of layer (4) for 120 min, where the spinel, PbFe, PCSi, and glass phases are indicated. The scale bars indicate the distance to the probe.

order of formation, spinel, PbFe, and PCSi crystals. Layer (4) is observed in all microstructures and is always in contact with the bath. Here, the spinel crystals formed before the PbFe crystals. Only at 120 minutes are no PbFe crystals observed at the bath–freeze-lining interface. In all microstructures, a thin layer (6) is observed.

Figure 7 shows the 5-, 60-, and 120-minute microstructures for the S2. At 120 minutes, five layers ((1) and (2) and (4) through (6)) are distinguished. These layers formed similar as for M2, except no layer (3) is observed. At 1 minute, layer (2) contains only spinel crystals, while from 5 minutes, melilite crystals and, from 30 minutes, PbFe-Si²⁺ crystals are also observed. Layer (4) is observed from 5 minutes. Although spinel

forms first, melilite is the dominant phase. After 30 minutes, PbFe-Si²⁺ crystals are also present at the probe side of this layer (4). Layer (5) is observed after 60 minutes and is dominated by melilite crystals. After 120 minutes, spinel is the dominant phase at the bath side of this layer (5).

For S3, the freeze lining consists of layers (1) and (6) during the first 60 minutes. No interface between the layers could be determined. After 60 minutes, some spinel crystals appear and layer (2) is observed between layers (1) and (6) (Figure 8). Because these crystals are only observed at a constant distance to the probe, it seems unlikely that they are present in the bath. Thus, they are assumed to be formed in glass or high-viscosity

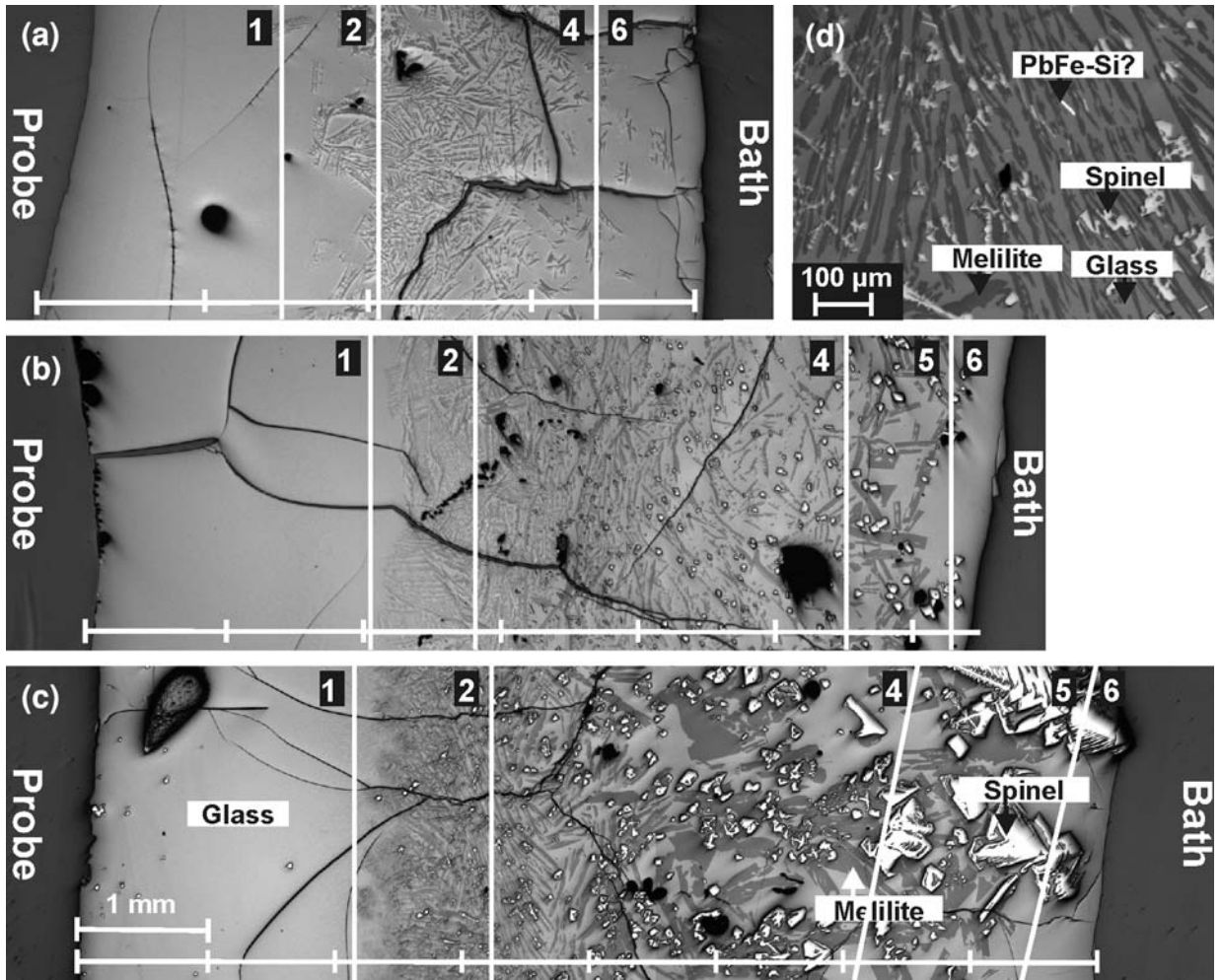


Fig. 7—LOM image of the freeze-lining microstructure of S2 after (a) 5, (b) 60, and (c) 120 min. Five layers ((1), (2), and (4) through (6)) are observed. Figure 7(d) shows a detail of the microstructure of layer (4) for 120 min in which the melilite, spinel, PbFe-Si?, and glass phases are indicated. The scale bars indicate the distance to the probe.

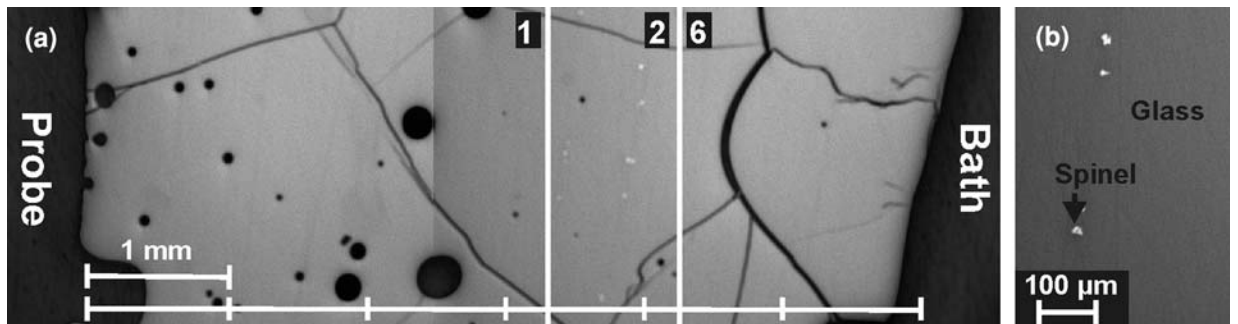


Fig. 8—LOM image of the freeze-lining microstructure of S3 after 120 min. Three layers ((1), (2), and (6)) are observed. Figure 8(b) shows a detail of the microstructure of layer (2) for 120 min in which the spinel and glass phases are indicated. The scale bars indicate the distance to the probe.

liquid, because, otherwise, they would not be attached to the freeze lining.

3. Composition of the slag bath

The initial bath compositions of the slags are shown in Table III. They slightly differ from the targeted bath

compositions. For all slags except S1, the EPMA analysis is considered to give the best analysis for the bath composition; the XRF analysis is not shown. For S1, the EPMA analysis seems to give rather low ZnO and Fe₂O₃ concentrations in the slag compared to the targeted composition in Table I. This deviation cannot

Table III. Composition of Initial Baths for Synthetic Lead Slags (Weight Percent); for All Slags, Results of EPMA Analysis Are Shown; Only for S1 Are the Results of the XRF Analysis Also Shown

| Initial Bath | CaO | SiO ₂ | PbO | ZnO | Fe ₂ O ₃ | Al ₂ O ₃ |
|--------------|-------|------------------|-------|------|--------------------------------|--------------------------------|
| M1 | 10.57 | 13.81 | 45.79 | 3.28 | 20.28 | 6.27 |
| M2 | 11.53 | 19.12 | 47.28 | 7.81 | 11.73 | 2.53 |
| M3 | 15.71 | 27.58 | 37.62 | 4.88 | 10.02 | 4.19 |
| S1 EPMA | 3.97 | 13.47 | 60.09 | 1.26 | 15.48 | 5.74 |
| S1 XRF | 3.70 | 9.56 | 55.80 | 4.44 | 21.35 | 4.90 |
| S2 | 12.88 | 23.82 | 42.58 | 6.69 | 10.34 | 3.69 |
| S3 | 7.78 | 28.58 | 45.98 | 3.61 | 8.83 | 5.21 |

be explained by volatile components or dissolution of the crucible material. The S1 easily crystallizes and, due to the formation of crystals, the glass composition deviates from the actual bath composition. Therefore, a bulk analysis with XRF is considered to be more accurate. The equilibrium solidification paths of the slags are shown in Figure 9. For Mx, melilite is never predicted to be the primary phase; spinel is. However, the melilite formation temperature is predicted to be close to the liquidus temperature and spinel is only predicted to be stable at high and low temperatures; the liquidus temperature is predicted to be a bit higher than 1200 °C (still lower than the bath temperature). For the Sx, spinel is predicted to be the primary phase and the liquidus temperature is predicted to be higher than the bath temperature. Note that the temperature at which melilite is predicted to form differs for Sx.

IV. DISCUSSION

Before evaluating the performance of the freeze linings for the studied slags, their microstructures are interpreted to determine the corresponding freeze-lining formation mechanisms. By studying the impact of each freeze-lining formation mechanism on freeze-lining growth, the influence of slag properties is discussed. Next, microstructural characteristics for a protective freeze lining are indicated and the freeze-lining formation of the slags is evaluated. Finally, the implications for freeze-lining applications are discussed.

A. Freeze-Lining Formation Mechanisms

1. Freeze-lining microstructure evolution

The freeze-lining formation of M2 is first discussed, because it has already been studied in previous research.^[11,12] The growth of the freeze lining is most likely dominated by the formation of a glass/high-viscosity liquid layer only during the first seconds (minute) because, at 1 minute, a crystals-in-liquid layer (4) is already observed in the freeze lining. The further growth is controlled by the growth of melilite crystals. After 30 minutes, the growth of sealing crystals of melilite and spinel phase controls the growth of the freeze lining. Their growth seems to depend on mass exchange between freeze lining and bath. The temperature at 1 cm from the probe, which is measured close to

the bath–freeze-lining interface, is relatively close to the liquidus temperature of the slag. Because the liquidus temperature is the maximum temperature at which crystals can form, above this temperature a solid layer is not stable. Therefore, the freeze lining of M2, although still growing, is assumed to be close to its steady-state thickness at 120 minutes. Eventually, a layer of only spinel crystals (primary phase) may form at the bath–freeze-lining interface.

For S3, the formation of a glass/high-viscosity liquid layer dominates the freeze-lining growth for a much longer time. Although some crystallization occurs after 60 minutes, these crystals do not interlock and their growth does not contribute to the freeze-lining growth. At 120 minutes, the temperature at 1 cm is approximately 1050 °C and the freeze-lining thickness is 6 mm. As a result, the liquid in front of the freeze lining is below the liquidus temperature and, with time, crystal growth can result in the further growth of the freeze lining.

During the first 60 minutes, the formation of a glass/high-viscosity layer also dominates the freeze-lining growth for M3. After 60 minutes, however, melilite crystals nucleate and grow large, resulting in the further growth of the freeze lining. This change in the freeze-lining growth mechanism results in a change in the freeze-lining growth rate (Figure 2(a)).

Initially, the freeze-lining growth for S2 is determined by the formation of a glass/high-viscosity liquid layer. After 1 minute, spinel crystals form at the hot side of this layer. However, the freeze lining does not seem to grow further until melilite crystals form between 1 and 5 minutes. At 60 minutes, the melilite crystals at the bath–freeze-lining interface have grown large and form a sealing-crystals layer (5). Between 60 and 120 minutes, the growth of the freeze lining is determined by the growth of spinel crystals only. The temperature at 1 cm from the probe shows that the freeze lining has not yet reached steady state; thus, with time, this spinel layer may grow thicker and denser.

M1 crystallizes very easily. For the first 30 to 60 minutes, the growth of the freeze lining occurs similar to M2. However, for M1, the overall temperature in the freeze lining is lower (for example, at 1 cm from the probe, the temperature for M1 is 900 °C at 120 minutes, while for M2, it is 1130 °C). After the formation of a melilite sealing-crystals layer, the spinel crystals start to dominate this layer at the bath side. This might be explained by a local change in composition at the bath–freeze-lining interface due to the growth of the large melilite crystals (depletion in melilite-forming components such as ZnO and CaO and enrichment in spinel-forming components such as Fe₂O₃), resulting in the formation of spinel crystals as primary phase instead of melilite. However, note also that other mechanisms such as particle pushing might (partly) cause the formation of this spinel-rich layer. Between 30 and 60 minutes, crystals start to interlock in the liquid in front of the sealing-crystals layer (5) and a second crystals-in-liquid layer (7) forms. The formation of this layer can be explained by the slow growth of the sealing-crystals layer due to the local depletion in spinel- and

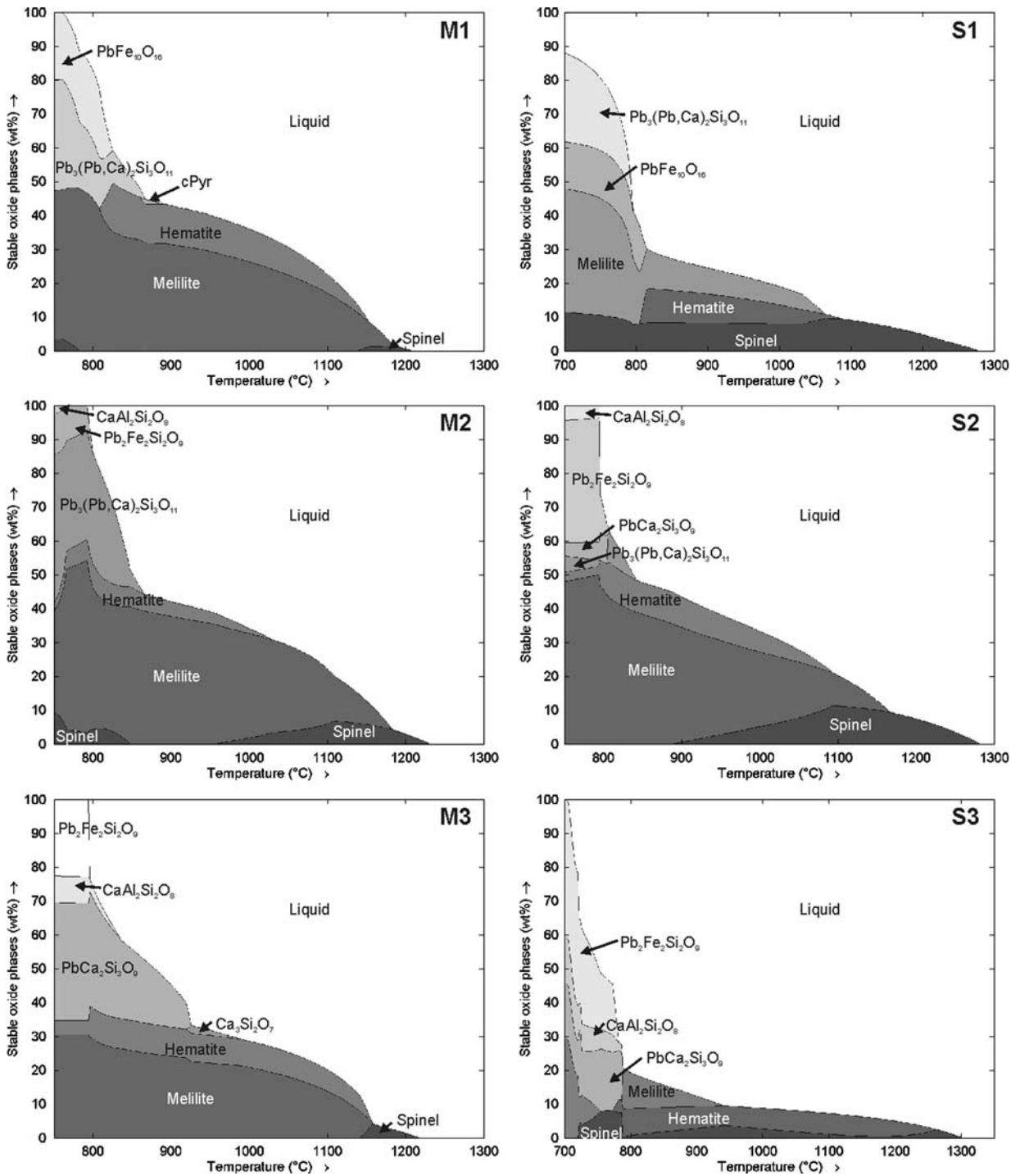


Fig. 9—Solidification paths of the initial bath for the slags, as predicted by FactSage. The composition data in Table III are used, using the XRF data for S1. cPyr (clinopyroxene) is a $\text{MSiO}_3\text{-MAI}_2\text{SiO}_6\text{-MFe}_2\text{SiO}_6$ solution ($\text{M} = \text{Fe}^{2+}, \text{Ca}, \text{Mg}$).

melilite-forming components (note the large fraction of glass phase at the probe side of the second crystals-in-liquid layer). As a result, the liquid in front of the sealing-crystals layer seems to be undercooled (at 1 cm, the temperature is approximately 950 °C at 60 minutes, which is far below the liquidus temperature) to such a degree for such a time that a network of crystals forms in this liquid, resulting in the further growth of the

freeze lining by changing the growth mechanism. The freeze lining of this slag has not reached steady state after 120 minutes.

S1 behaves differently from the other slags. It also rapidly crystallizes; thus, the formation of a glass/high-viscosity liquid layer only shortly dominates the freeze-lining growth. However, the further growth is largely dominated by the PbFe phase and not by the melilite

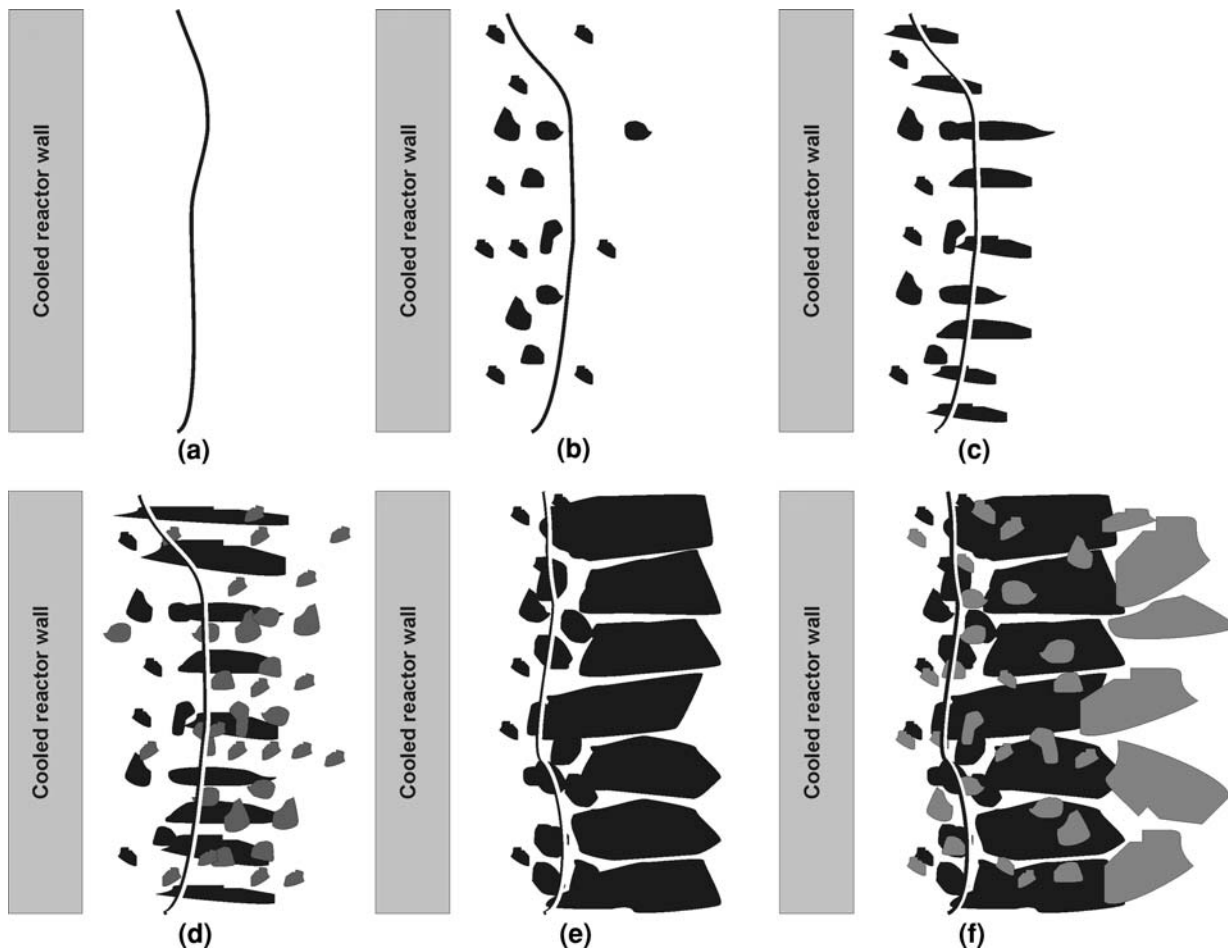


Fig. 10—Schematic representation of different stages in freeze-lining growth: (a) a glass/high-viscosity layer, (b) non-interlocking crystals in the glass/high-viscosity layer, (c) interlocking crystals in the glass/high-viscosity layer resulting in the formation of a crystals-in-liquid layer, (d) a crystals-in-liquid layer containing low-melting interlocking crystals and high-melting non-interlocking crystals, (e) the sealing-crystals layer of a high-melting interlocking phase, and (f) a high-melting phase layer formed after the crystals-in-liquid layer is formed with interlocking crystals differ from the high-melting phase.

phase. After 30 minutes, the layer with PbFe crystals seems to have reached its maximum thickness. The stoppage of the PbFe crystal growth might be explained by the relative low formation temperature of the phase (approximately 810 °C, according to Figure 9(b)). The slag in front of the freeze lining is far below the liquidus temperature (the temperature at 1 cm is 860 °C after 120 minutes) and contains several spinel crystals. Most of the spinel crystals, however, seem to “swim” in the liquid in contact with the freeze lining, where they can easily be washed away and they do not form a part of the freeze lining.

2. Influence of slag properties

The interpretation of the microstructure evolution suggests that similar freeze-lining formation mechanisms occur for all slags. The period during which they primarily dominate the freeze-lining growth seems to differ for each slag. This can be explained by the difference in the slag properties of the studied slags.

First, a glass or a high-viscosity liquid layer forms, as is shown in Figure 10(a). At this moment, the growth of the freeze lining is determined by heat transfer, because

all the slag at the reactor wall that is below the glass-transition temperature or below the transition temperature between high- and low-viscosity slag is part of the freeze lining. Thus, the glass-transition temperature, the viscosity-temperature relation of the slag, and the crystallization behavior of the slag affect the freeze-lining formation. Note that the glass-transition temperature and the viscosity-temperature relation are mentioned separately because, for some slags, the viscosity of the slags strongly decreases above the glass-transition temperature, while for other slags, it only slightly decreases just above the glass-transition temperature and the liquid is rather immobile. For M3 and S3, the freeze-lining growth seems to be dominated for a long time by the formation of a glass/high-viscosity liquid layer. These slags have the highest SiO₂ concentration and, thus, the highest viscosities and a lower mobility of the atoms.

To grow further, it seems to be important that crystals form and interlock, as is illustrated by the microstructure evolutions of M3 and S3. For the S3, spinel crystals form in the glass/high-viscosity liquid layer, but they do not interlock (Figure 10(b)). As a result, the

freeze-lining growth is still dominated by heat transfer. For M3, melilite crystals grow large and interlock, resulting in the further growth of the freeze lining (Figures 10(c) and (d)). For M1, M2, M3, and S2, melilite is the interlocking phase; for S1, PbFe crystals interlock. The spinel crystals form first for most slags. However, these crystals do not seem to contribute to the growth of the freeze lining, but seem to be entrapped by the interlocking phases. Only in the sealing-crystals layer of S2 does the spinel seem to contribute to the growth of the freeze lining. Thus, the ability of a phase to interlock and contribute to the freeze-lining growth might depend on local conditions. Furthermore, the stability temperature range of the interlocking crystals seems to be important. For S1, the freeze lining seems to stop growing as the bath–freeze-lining interface temperature approaches the PbFe formation temperature. No other phase seem to interlock: The attachment of the spinel crystals to the freeze lining or their growth seems to occur very slowly.

Previous research indicated that mass transfer is also important for freeze-lining growth.^[10,11] At the hot side of the freeze lining, large crystals that grow slowly are present. These crystals differ in composition from the bath and their growth seems to be dominated by the mass exchange between the bath and freeze lining. For example, in the microstructure of S2, the spinel crystals in the sealing-crystals layer differ strongly in composition from the bath. As a result, extensive mass exchange between the bath and freeze lining is necessary for these crystals to grow large.

Furthermore, the temperature at 1 cm strongly differs for the slags: For example, after 120 minutes, temperatures of approximately 1050 °C and approximately 860 °C are recorded for M2 and S1, respectively. This indicates that these slags have different heat conductivities. In the literature, it is mentioned that the presence of Fe²⁺ affects the heat conductivity of a slag, because heat can be transferred by conduction electrons.^[17] About the presence of Fe³⁺, nothing is mentioned, however; this component may behave similarly (certainly in the presence of a small amount of Fe²⁺). Furthermore, the disordering of the silicate network by basic oxides is thought to affect the heat conductivity; a higher disordering gives a lower thermal conductivity.^[18] This effect, however, is found to be minimal for high values of slag basicity. For M2 and S1, the difference in heat conductivity could be explained by the domination of the effect of Fe. The heat conductivity of the slag is thus also important: A direct result of an increase in heat conductivity is the formation of a thicker freeze lining.

B. Evaluation of Performance of Studied Slags as a Protective Freeze Lining

1. Indication of microstructural characteristics for a protective freeze lining

Before evaluating the freeze-lining behavior of the studied slags, the microstructural characteristics of a protective freeze lining have to be indicated. A freeze lining can be considered to protect the reactor wall, if it

limits the contact between the reactor wall and the corrosive process material and if it remains stable during changes in process conditions such as bath composition and bath temperature. Should this stable layer consist of glass/high-viscosity liquid or crystals? The growth of a glass/high-viscosity liquid layer is determined by the temperature distribution in the process material at the reactor wall. The disadvantage of such a freeze lining is that it easily disappears at increasing temperatures. Furthermore, the glass formation temperature can be roughly estimated at 2/3 of the liquidus temperature.^[19] Because the bath temperature is often close to or higher than the liquidus temperature, the glass formation temperature is often far below the bath temperature. As a result, the heat losses will be high and the cooling capacity of the furnace has to be high. Also, the freeze-lining thickness increases if the temperature at the bath–freeze-lining interface increases for similar conditions (Figure 11). Therefore, a freeze lining will most likely give better protection if the temperature at the bath–freeze-lining interface is close to the bath temperature and if the shrinking of the freeze lining does not depend only on a change in temperature. This can be obtained by the formation of a freeze lining that contains large crystals at the bath–freeze-lining temperature that are in equilibrium with the bath in a temperature range around the targeted bath temperature (the larger this range, the better), the composition of which differs from the bath composition. The difference in composition might slow down the “melting” of the crystals because mass transfer is needed, which implies that the crystals must “dissolve” in the bath. Solheim *et al.* show that, in the case of cryolite salt, this will slow down the melting process of the freeze lining.^[5,20]

A freeze lining should form rapidly, to limit the contact between the refractory wall and the bath material. The formation of the desired high-melting crystalline layer may take time, because mass exchange is needed. To obtain rapid freeze-lining formation, the crystals should form rapidly and interlock, resulting in the formation of a crystals-in-liquid layer. These interlocking crystals should be stable at sufficiently high temperatures, in order to form high-melting crystalline crystals at the bath side of the crystals-in-liquid layer, which form some time after the desired protective high-melting crystalline layer. Thus, initially, a freeze lining as shown in Figures 10(c) or (d) should form rapidly and, with time, this freeze lining should grow further to form a high-melting crystalline layer, as is shown in Figures 10(e) or (f). The time in which this high-melting crystalline layer should form should be lower than the time it takes for the bath to change temperature or composition, resulting in the “wear” of the freeze lining, and is thus defined by the process conditions.

Thus, to protect the reactor wall, a freeze lining should form rapidly, to limit the contact between the reactor wall, and should remain stable during changes in heat input from the bath and in the bath composition. These demands can be fulfilled if the initial growth of a freeze lining is determined by the rapid formation and steady growth of interlocking crystals and the subsequent formation of a high-melting crystalline layer that is in

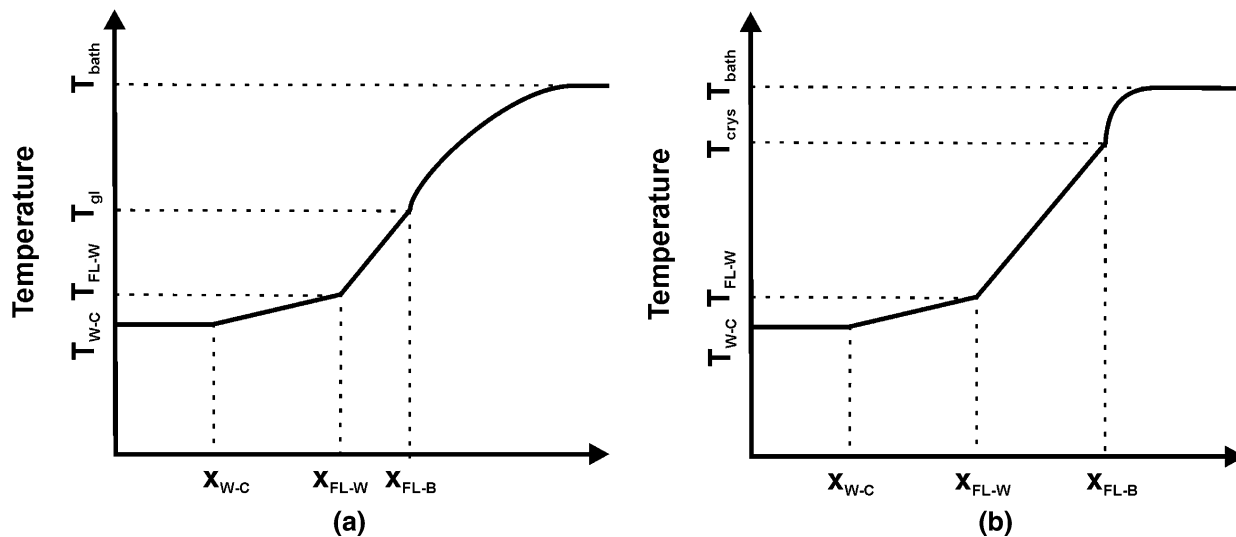


Fig. 11—Schematic representation of the temperature profile in a freeze lining with (a) glass and (b) crystals at the bath–freeze-lining interface. T_{bath} is the bath temperature and $T_{\text{W-C}}$ and $T_{\text{FL-W}}$ are the temperature at the wall–cooling system and at the freeze-lining–wall interfaces, respectively, T_{crys} is the crystal formation temperature, T_{gi} is the glass-transition temperature, and $x_{\text{W-C}}$, $x_{\text{FL-W}}$, and $x_{\text{FL-B}}$ indicate the positions of the wall–cooling-system, freeze-lining–wall, and freeze-lining–bath interfaces, respectively. Note that T_{gi} is lower than T_{crys} and that the distance between $x_{\text{FL-W}}$ and $x_{\text{FL-B}}$ in (b) is higher than in (a).

equilibrium with the bath material at a temperature range around the bath temperature and of which the composition differs sufficiently from the bath composition.

2. Evaluation of the studied slags

According to the proposed microstructural characteristics, M3 and S3 form the worst freeze linings, because the formation of a glass/high-viscosity liquid layer dominates their freeze-lining growth for a relatively long time. The other slags rapidly form a freeze lining containing interlocking crystals and, thus, seem to meet the demand of rapid freeze-lining formation. For S1, a stagnation of the growth is observed, because the bath–freeze-lining temperature seems to be too high for the PbFe crystals to grow further. Although spinel crystals are present in the entrained-bath layer, they do not form a sealing-crystals layer within the experiment time of 120 minutes. As a result, S1 seems to be less effective in forming a protective freeze lining than M1, M2, or S2. These slags rapidly form a layer of a certain thickness containing interlocking crystals and, with time, grow a sealing-crystals layer that contains both melilite and spinel crystals. Thus, with time, a high-melting-phase layer forms at the bath–freeze-lining interface. As a result, these slags may be considered to form a protective freeze lining. M2 and S2 form this sealing-crystals layer at the hot side of the freeze lining. M1, however, already forms such a layer at a cold part of the freeze lining. Because the M1 freeze lining, contrary to the M2 and S2 freeze linings, is not close to its steady-state thickness; more such sealing-crystals layers can appear in the freeze lining and they might grow thicker than for the other slags. Therefore, this slag might contain multiple “high-melting” layers and might form the best protective freeze lining of all the studied slags.

Note that the previous reasoning is still hypothetical and the stability of these high-melting layers should be further validated with experiments.

C. Implications for Freeze-Lining Applications

The present results show that slag properties can strongly influence freeze-lining formation. Therefore, it is important to consider slag engineering whenever freeze-lining technology is applied. By changing slag properties such as viscosity, the type of crystalline phases, the temperature range in which a phase is stable, and the crystallization behavior, the freeze lining formation rate can be influenced and the freeze lining stability can be controlled. In reality, a certain process window has to be considered, to optimize both process conditions and stable freeze-lining formation. Note that slag engineering might not always be possible: For ilmenite smelting, the slag is the end product and additions might be unwanted.^[21]

The present research focuses on freeze-lining formation. No bath–freeze-lining interactions due to change in the bath temperature or composition are studied. These should also be investigated in order to fully understand what constitutes a stable freeze-lining formation.

V. CONCLUSIONS

In order to illustrate the importance of slag engineering when using freeze linings, the freeze-lining formation of six synthetic lead slags has been studied. These slags vary in spinel and melilite formation temperatures and in SiO_2 concentration. The results show that the slag properties affect the period during which a certain freeze-lining formation mechanism, such as the

formation of a glass/high-viscosity liquid layer, the growth of interlocking crystals, or the mass exchange between the bath and freeze lining, dominates the freeze-lining growth. The relevant properties for the studied slags seem to be the viscosity, the crystallization behavior, the type of phases formed (interlocking or not), and the temperature range over which a phase is stable.

To protect the reactor wall, a freeze lining should form rapidly to limit the contact between the reactor wall and should remain stable during changes in heat input from the bath and in the bath composition. For a freeze lining in continuous contact with a slag bath, these demands can be fulfilled if the initial growth of a freeze lining is determined by the rapid formation and the steady growth of interlocking crystals and the subsequent formation of a high-melting crystalline layer finally that is in equilibrium with the bath material at a temperature range around the bath temperature and of which the composition differs sufficiently from the bath composition.

For the studied slags, melilite and $\text{PbFe}_{10}\text{O}_{16}$ form interlocking crystals and spinel does not. The rapid formation of a protective freeze lining seems to be optimal when melilite is stable within a large temperature range, with the maximum stability temperature close to the liquidus temperature, and for relatively low SiO_2 concentrations in the slag.

ACKNOWLEDGMENTS

The authors thank Umicore (Olen, Belgium) for its financial support and, in particular, Maurits Van Camp, Luc Coeck, Tim Van Rompaey, Saskia Bodvin, Danny Leysen, Marc Bakelants, Eddy Boydens, Ann Van Gool, and Greet Peeraer for valuable discussions, support with the probe experiments, and characterization.

REFERENCES

1. K.A. Rye, T. Eidet, and K. Tørklep: *Light Metals 1999*, TMS, Warrendale, PA, 1999, pp. 347–52.
2. C.C. Wei, J.J.J. Chen, B.J. Welch, and V.R. Voller: *Light Metals 1997*, TMS, Warrendale, PA, 1997, pp. 309–16.
3. D.G.C. Robertson and S. Kang: *Fluid Flow Phenomena in Metals Processing*, TMS, Warrendale, PA, 1999, pp. 157–68.
4. J. Thonstad and S. Rolseth: *Light Metals 1983*, TMS-AIME, Warrendale, PA, 1983, pp. 415–23.
5. A. Solheim and L.I.R. Støen: *Light Metals 1997*, TMS, Warrendale, PA, 1997, pp. 325–32.
6. K. Verscheure, M. Van Camp, B. Blanpain, P. Wollants, P. Hayes, and E. Jak: *Metall. Mater. Trans. B*, 2007, vol. 38B, pp. 13–20.
7. K. Verscheure, M. Van Camp, B. Blanpain, P. Wollants, P. Hayes, and E. Jak: *Metall. Mater. Trans. B*, 2007, vol. 38B, pp. 21–33.
8. K.C. Mills, S.U. Yuchu, A.B. Fox, Z. Li, R.P. Thackray, and H.T. Tsai: *ISIJ Int.*, 2005, vol. 45 (5), pp. 619–33.
9. M. Campforts, K. Verscheure, E. Boydens, T. Van Rompaey, B. Blanpain, and P. Wollants: *Metall. Mater. Trans. B*, 2007, vol. 38B, pp. 841–51.
10. M. Campforts, K. Verscheure, E. Boydens, T. Van Rompaey, B. Blanpain, and P. Wollants: *Metall. Mater. Trans. B*, 2008, vol. 39B, pp. 408–17.
11. M. Campforts, E. Jak, B. Blanpain, and P. Wollants: *Metall. Mater. Trans. B*, 2009, vol. 40B, Doi: [10.1007/s11663-009-9256-9](https://doi.org/10.1007/s11663-009-9256-9).
12. M. Campforts, E. Jak, B. Blanpain, and P. Wollants: *Metall. Mater. Trans. B*, 2009, vol. 40B, Doi: [10.1007/s11663-009-9257-8](https://doi.org/10.1007/s11663-009-9257-8).
13. K. Verscheure, M. Campforts, F. Verhaeghe, E. Boydens, M. Van Camp, B. Blanpain, and P. Wollants: *Metall. Mater. Trans. B*, 2006, vol. 37B, pp. 929–40.
14. C.W. Bale, P. Chartrand, S.A. Degterov, G. Eriksson, K. Hack, R. Ben Mahfoud, J. Melançon, A.D. Pelton, and S. Petersen: *Calphad*, 2002, vol. 26 (2), pp. 189–228.
15. S. Degterov, I.H. Jung, E. Jak, P. Hayes, and A.D. Pelton: *Proc. VII Int. Conf. on Molten Slags, Fluxes and Salts*, SAIMM, Johannesburg, South Africa, 2004, pp. 839–50.
16. E. Jak, S. Degterov, B. Zhao, A.D. Pelton, and P.C. Hayes: *Metall. Mater. Trans. B*, 2000, vol. 31B, pp. 621–30.
17. Verein Deutscher Eisenhüttenleute: *Slag Atlas*, 2nd ed., Verlag Stahleisen GmbH, Düsseldorf, Germany, 1995, pp. 591–99.
18. R. Eriksson, M. Hayashi, and S. Seetharaman: *Int. J. Thermophys.*, 2003, vol. 24 (3), pp. 785–97.
19. W. Kauzmann: *Chem. Rev.*, 1948, vol. 43 (2), pp. 219–56.
20. A. Solheim: *12th Aluminium Symp.*, Bratislava, Slovakia, 2003.
21. P.C. Pistorius: *J. S. Afr. Inst. Min. Metall.*, 2008, vol. 108 (1), pp. 35–43.